Contents lists available at GrowingScience

Current Chemistry Letters

homepage: www.GrowingScience.com

Theoretical and computational study of tannin adsorption on wood surface particularly on β-cellulose

El hassan El -Karni[a], Zakaria Jalil[a], Mohamed Amine Kasbaji[a], Meriem Kasbaji[a], M'hamed Touil[b], Amine Moubarik[c], Omar Bajjou[a,d], Mohamed M'barki[a] and Mustapha Oubenali[a*]

[a]*Engineering in Chemistry and Physics of Matter Laboratory, Faculty of Science and Technologies, Sultan Moulay Slimane University, PB: 523, Beni Mellal, Morocco*
[b]*Materials Science and Sustainable Energy Laboratory, Department of Chemistry, Faculty of Science, Abdelmalek Essaadi University, B.P. 2121, M'Hannech II, 93030 Tétouan, Morocco*
[c]*Chemical Processes and Applied Materials Laboratory, Polydesciplinary Faculty, Sultan Moulay Slimane University, PB: 592, Beni Mellal, Morocco*
[d]*UNESCO UNISA Africa Chair in Nanosciences & Nanotechnology (U2ACN2), College of Graduate Studies, University of South Africa (UNISA), Pretoria, South Africa*

C H R O N I C L E

Article history:
Received October 2, 2024
Received in revised form
November 1, 2024
Accepted January 31, 2025
Available online
January 31, 2025

Keywords:
Adsorption
Tannins
Cellulose
CDFT
NBO Analysis

A B S T R A C T

This theoretical study investigates the adsorption of eco-friendly tannins on cellulose surfaces as a means to develop sustainable wood adhesives with reduced formaldehyde emissions. Conceptual density functional theory calculations reveal the global and local chemical reactivity parameters governing the interaction between tannins and wood substrates. Monte Carlo simulations explore the configuration space of substrate adsorbate, while molecular dynamics simulations elucidate the binding strength and stability of tannins. The results demonstrate that tannins adsorb parallel to the cellulose surface, driven by donor-acceptor interactions. The adsorption energy calculations reveal spontaneous adsorption, with prodelphinidin exhibiting the strongest adsorption energy. This research provides valuable insights into the adsorption behavior of tannins and contributes to the development of eco-friendly wood adhesives that mitigate formaldehyde emissions.

1. Introduction

The demand for environmentally friendly wood adhesives in the wood industry is increasing due to environmental concerns and the urgent need for sustainable alternatives[1]. Traditional synthetic wood glues, while popular for their affordability, fast curing time, and strong bonding properties, have significant disadvantages due to the release of toxic formaldehyde during and after application[1–4]. To address this issue, the researchers turned their attention to the potential of tannins as additives with the goal of reducing harmful formaldehyde emissions and reducing production costs associated with formaldehyde-based wood adhesives[5–9].

In this context, the present article contributes to the body of knowledge with a comprehensive theoretical study focusing on the adsorption behavior of tannins on cellulose surfaces, commonly found in wood materials. The study uses advanced computational methods, in particular conceptual density functional theory (CDFT)[10], to delve into the intricate details of three distinct molecules of tannin compounds, namely procyanidin, profisetidin, and prodelphinidin.

Conceptual density functional theory calculations have proven to be a powerful tool for assessing the stability and reactivity of molecules. Using conceptual density functional theory, researchers can investigate the stability and reactivity of tannins by examining global and local descriptors of chemical reactivity[11,12]. These descriptors provide valuable

* Corresponding author
E-mail address mustapha.oubenali@gmail.com (M. Oubenali)

doi: 10.5267/j.ccl.2025.1.005

information on electronic structure, molecular frontier orbitals and provide information on charge transfer between tannin molecules and their wood surface counterparts. Using natural bond orbital (NBO) analysis and CDFT methods, we perform calculations to determine the electron density (ED) distribution and E(2) energy in different bonding and antibonding orbitals. These calculations provide convincing evidence of the stability resulting from hyperconjugation in various intramolecular interactions.

The adsorption of tannins onto wood surfaces, in particular cellulose (β-Cellulose)[13], was investigated using complementary calculations that were performed in addition to CDFT calculations. The first method included statistical thermodynamic calculations based on Monte Carlo (MC) simulations, and the second method included molecular dynamics (MD) simulations. The results of these simulation tools provide insight into bond energy distributions, adsorption configurations, and implications for the development of a sustainable wood adhesive.

In conclusion, this theoretical study combines the capabilities of conceptual density functional theory and global and local chemical reactivity descriptors to investigate in detail the stability and reactivity of different tannin molecules. By examining their behavior on cellulose surfaces, this research makes a significant contribution to understanding their potential as non-polluting additives in wood adhesive formulations. Ultimately, the results of this study promise to advance the development of more environmentally friendly and safer wood adhesives in the industry, in line with the growing demand for sustainable practices and environmentally friendly solutions.

2. Computational Methods

The Gaussian computer program is widely used by scientists, including chemists, chemical engineers, biochemists, physicists, and many others. Based on the fundamental laws of quantum mechanics[14], Gaussian lets you predict the energies, molecular structures, vibrational frequencies, and chemical properties of complex molecular systems[11,12,15–17]. Molecules and reactions can be studied under a wide range of conditions, not only for stable species or complex compounds but also for experimentally unobservable compo. We employed the CDFT approach with the B3LYP functional, which combines Becke's three-parameter hybrid functional with Lee-Yang-Parr correlation functional theory[18–20], to optimize the geometries of all the molecules. The spherical basis set 6-311G (d, p) was used for the calculations. The B3LYP functional with the 6-311G (d,p) basis set has been chosen for several reasons. One of these reasons is that it provides a good balance between accuracy and computational efficiency; this combination generally offers a good compromise between result precision and computation time. The 6-311G (d,p) basis set is sufficiently flexible to adequately describe the electron distribution of many molecules, while remaining computationally affordable. Additionally, the 6-311G (d,p) basis set uses a triple-zeta description for the valence orbitals, meaning they are described by three sets of Gaussian functions. This allows for a better representation of the electronic correlation effects in the valence region[21-23].

To study the reactivity of three molecules of tannin compounds, namely procyanidin, profisetidin, and prodelphinidin, various energy parameters were calculated. These include the energy of the highest occupied molecular orbital (HOMO), the energy of the lowest unoccupied molecular orbital (LUMO), the energy gap between LUMO and HOMO (ΔE), the dipole moment (D) and the electron affinity (EA). These calculations provide insight into the reactivity of the compounds studied.

Global reactivity descriptors are used to evaluate the overall reactivity of a chemical compound. The global parameters used in this study, which is based on CDFT, are electronegativity (χ), chemical potential (μ), global hardness (η), global softness (S), maximum charge transfer (ΔN_{max}), global electrophilicity index (ω), global nucleophilicity index (Nu), Dipole Moment and Polarizability (α). The IP and EA parameters can be substituted by the frontier orbital energy by the following Eq. (1) Eq. (2)[24–27].

$$\mathrm{IP} = -E_{HOMO} \tag{1}$$

$$\mathrm{EA} = -\mathrm{E_{LUMO}} \tag{2}$$

The key concept in the CDFT approach is electronegativity, which can be defined as the first derivative of energy (E) with respect to the total number of electrons N. Parr and Pearson demonstrated that the second derivative of energy is equal to the negative value of the chemical potential, as shown by relation (3)[28].

$$\chi = -\mu = -\left(\frac{\partial \mathrm{E}}{\partial \mathrm{N}}\right)_{\mathrm{V}(\vec{\mathrm{r}})} \tag{3}$$

Eq. (4) can be used to provide the operational equations for calculating these two parameters by using the method of finite differences[15,16,29].

$$\chi = -\mu \simeq \frac{1}{2}(\mathrm{IP} + \mathrm{EA}) \tag{4}$$

According to Eq. (5)[30], the global hardness, or second derivative of energy *E* with respect to *N*, is a crucial variable for comprehending structure and reactivity.

$$\eta = \left(\frac{\partial^2 E}{\partial N^2}\right)_{V(\vec{r})} = \left(\frac{\partial \mu}{\partial N}\right)_{V(\vec{r})} \tag{5}$$

the nucleophilicity N′ index as the inverse of Gázquez' selectrodonating ω^- power[31].

$$N' = \frac{10}{\omega^-} \tag{6}$$

In a recent study, Gázquez et al[32]. established the electroaccepting power (as indicated in Eq. (7)), denoted as $\omega+$, and the electrodonating power (as shown in Eq. (8)), represented as ω:

$$\omega^- = \frac{EA^2}{2(IE - EA)} \tag{7}$$

$$\omega^+ = \frac{EA}{2(IE - EA)} \tag{8}$$

Global softness (S) is a term used to represent the opposite side of hardness. Equations (9) and (10) can be used to calculate S and η[33].

$$\eta \simeq \frac{1}{2}(\mathrm{IP} - \mathrm{EA}) \tag{9}$$

$$\mathrm{S} = \frac{1}{2\eta} \tag{10}$$

The electrophilicity index (w) measures the stabilization of energy when the system acquires an additional electronic charge from the environment. In fact, Parr et al [16,34–37] established the following Eq. (11) to calculate this parameter.

$$\omega = \frac{\mu^2}{2\eta} \tag{11}$$

According to the Kohn-Sham scheme[11,38–41], the empirical nucleophilic index is defined by the following equation.

$$\mathrm{Nu} = \mathrm{E}_{\mathrm{HOMO(Nu)}} - \mathrm{E}_{\mathrm{HOMO(TCE)}} \tag{12}$$

Tetracyanoethylene (TCE) is taken as a reference due to its lowest Highest Occupied Molecular Orbital (HOMO) energy in a large series of molecules. In this scale, the nucleophilic index of TCE is EHOMO (TCE) = -0.335198 Hartree, calculated with CDFT/B3LYP 6-311G (d, p).

Fukui functions[42,43] can be employed to determine the electron density after the addition or removal of electrons to determine the optimal attack site, or so-called regioselectivity in chemical reactivity . They can determine where the most electrophilic and nucleophilic regions are located in the molecule. The condensed Fukui function can be used to account for the local chemical reactivity of each atom[44–46]. It is then possible to determine the local softness. In this study, we applied DMol3to run the Fukui functions(f_k), and BIOVIA Materials Studio[47,48] was used to create the graphical representations. For nucleophilic attack and electrophilic attack, the following relations express them.

$$\mathrm{f}^+ \simeq |\Psi_{\mathrm{LUMO}}|^2 + 2\sum_{\mathrm{j}=1}^{\mathrm{HOMO}} \left(\frac{\partial |\Psi_{\mathrm{j}}(\mathrm{r})|^2}{\partial \mathrm{N}}\right)^+ \tag{13}$$

$$\mathrm{f}^- \simeq |\Psi_{\mathrm{HOMO}}|^2 + 2\sum_{\mathrm{j}=1}^{\mathrm{LUMO}} \left(\frac{\partial |\Psi_{\mathrm{j}}(\mathrm{r})|^2}{\partial \mathrm{N}}\right)^- \tag{14}$$

It has also been suggested to predict the local reactivity (site selectivity) of a chemical species using condensed local electrophilicity at atom k (ω_k) and condensed local nucleophilicity at atom k (N_k). The equation below provides these parameters.

$$N_k^- = N.f_k^- \tag{15}$$

$$\omega_k^+ = \omega . f_k^+ \quad (16)$$

To predict the local reactivity of a chemical species, several other local reactivity descriptors have been suggested. These include Parr functions (P_k), the local nucleophilicity at atom k (N_k), and the local electrophilicity index at atom k (ω_k). The corresponding equations for these parameters are provided in Eq. (17) and Eq. (18)[49-51].

$$N_K^- = N . P_K^- \quad (17)$$

$$\omega_K^+ = \omega . P_K^+ \quad (18)$$

3. Results and discussion

3.1. Global chemical reactivity descriptors and energetic parameters

To find the most stable conformation for every single component, we first optimized the molecular structures of three different molecules of tannin compounds, namely procyanidin, profisetidin and prodelphinidin. B3LYP/6-311G (d, p) in the gas phase and water as the solvent was employed to further refine the ideal conformation (**Fig.1**). Without any symmetry restrictions, the geometries of these molecules are all created for the singlet spin state. All stationary points were determined to be minima by a Hessian calculation using Gaussian software (no imaginary frequencies).

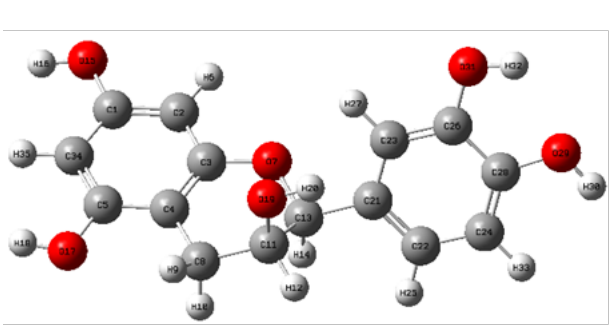

Procyanidin

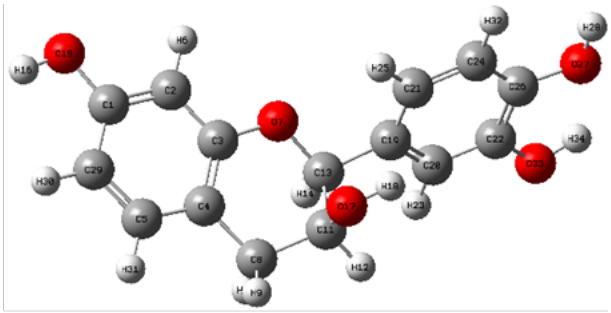

Profisetidin

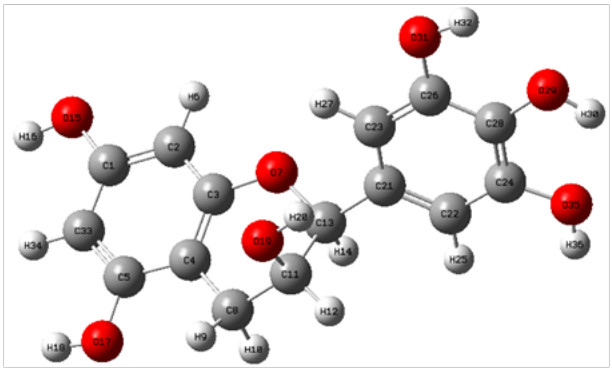

Prodelphinidin

Fig. 1.DFT/B3LYP optimized structures of Procyanidin, Profisetidin, and Prodelphinidin.

Adsorption is a surface phenomenon that occurs when atoms, ions, or molecules from a gas phase, liquid or solid solution bind to a solid surface. The interaction of the adsorbate with a surface, which may involve a variety of more or less intensive processes, including Van der Waals interactions, dipolar interactions, or covalent or ionic chemical bonds, forms the basis of the adsorption process.The latter, i.e. chemical bonds, are mainly due to the formation of donor-acceptor complexes on the surface of the adsorbent. σ-electron donation is based on donor-acceptor interactions between conjugated π-electrons or between unshared electron pairs of adsorbate heteroatoms and vacant atomic orbitals on the solid surface[52].

Numerous investigations have shown that the orbital interaction approach results from the physical and /or chemical interaction between an electrophile and a nucleophile that takes place when the HOMO (donor) and LUMO (acceptor) overlap. **Table 1** presents the energy parameters and global chemical reactivity descriptors of the Tannin derivatives in the

aqueous phase by using the conductor-like polarizable continuum model (CPCM)by means ofthe B3LYP/6-311G (d, p) method.

Table 1. Energetic parameters and Global chemical reactivity descriptors of the molecules.

Molecules	Procyanidin	Profisetidin	Prodelphinidin	β-Cellulose monomer
E_{HOMO} (eV)	-5.98	-5.97	-5.98	- 6.99
E_{LUMO} (eV)	-0.42	-0.43	-0.22	0.77
χ (eV)	3.20	3.20	3.10	3.11
μ (eV)	-3.20	-3.20	-3.10	-3.11
η (eV)	2.77	2.77	2.88	3.88
$S(\text{eV})^{-1}$	0.18	0.18	0.17	0.12
ω(eV)	0.92	0.92	0.83	0.62
ω^- (eV)	-3.21	-3.21	-3.10	-3.10
ω^+(eV)	0.01	0.01	0.00	0.59
N'(eV)	-3.11	-3.11	-3.22	-2.68
N_u(eV)	3.38	3.3898	3.38	2.37
Dipole Moment	**4.71**	**2.77**	**5.98**	**6.03**
Polarizability(α)	**241.87**	**237.26**	**247.18**	**212.41**
Molarvolume(cm^3/mol)	**192.35**	**175.47**	**221.36**	**206.64**

A detailed analysis of **Table 1** shows that the molecules studied have significantly different values for The polarity (dipole moment) and Polarizability (α) of the adsorbed molecules; The size of these molecules (molar volume). It should be noted that these parameters can affect the physical adsorption of a substance to support. In fact, the dipole moment is a measure of the asymmetry of the molecular charge distribution and the polarity of a polar covalent bond. It is defined as the product of the charge of the atoms and the distance between the two bonded atoms. It is principally used to study intermolecular interactions involving dipole-dipole forces of the Van der Waals type, because the greater the dipole moment, the stronger the intermolecular attraction , so a high value of dipole moment probably increases adsorption between a chemical compound and a substrate surface.The ability of the electron cloud to deform in response to an external electric field is quantified as polarisability. In chemical reactions, the most stable species (reactants or products) have the lowest sum of polarisability, whereas the most reactive species are those with the highest polarizability.When the contact surface between a molecule and the substrate is significant, molecules attach to surfaces more successfully. The strength of adsorption then increases as a result of the molar volume increasing contact.

by the electric dipole moments acting on each other. Each generates an electric field to which the other is subjected, producing two forces that work together to align the moments with each other[53,54]. The dipole moment and average polarizability (α) of the Prodelphinidin molecule are higher,respectively equal to (5.9879 D), (247.184 (ua)), which considerably increases its dipole-dipole interaction with the β-cellulose and leads to better adsorption on the β-cellulose surface. Based on our findings, it is evident that Prodelphinidin has the biggest molecular volume (221.361(cm^3/mol)), which raises the contact surface and, thus, the potential for adsorption onto the β-cellulose surface.This result leads us to propose that the interaction between these molecules derived fromtannins and the β-cellulose surface is electrostatic (physisorption). This interaction suggests that Columb interactions may be dominant and that interactions are governed by charge control.

The analysis of ω^- and ω^+ indicates that the β-cellulose molecule exhibits the highest electroacceptor capacity, as evidenced by its ω^+ value of 0.59 eV, which surpasses that of the other molecules. Conversely, the Prodelphinidin molecule demonstrates a greater electrodonor characteristic due to its significant ω^- value of -3.10 eV.In this work, we performed additional calculations to determine which interactions are responsible for the cohesion of the tannin-cellulose system. Chemoselectivity, NBO analysis, Monte Carlo simulation and molecular dynamics are used in these calculations.

3.2. Regioselectivity Index and NBO Analysis

3.2.1. Regioselectivity Index

Our molecular system has several reactive sites, and the reaction occurs selectively at one of these sites. We have used quantitative tools such as Fukui indices (f_k)and Parr indices (p_k), and qualitative tools such as chemical electrostatic potential (MEP) to analyze and evaluate the reactivity of different sites within the same chemical system. In order to comprehend the binding in this family of complexes (tannins-β-Cellulose), the potential for a close correlation between these interactions and the van der Waals penetration distance, and to study the presence of potent and stable intermolecular O-H---O interactions, natural bond orbital or NBO, have been calculated. Studies on the chemical reactivity or biological activity of a molecule can be conducted using the Molecular Electrostatic Potential (MEP), which offers comprehensive information. The binding of a substrate to the active site of a receptor is primarily governed by the three-dimensional distribution of the electrostatic potential. MEP is typically applied in the form of reactivity maps, which display the regions of organic molecules that are most vulnerable to electrophilic or nucleophilic attack by charged reactants.

In this study, we used the B3LYP/6-311G (d, p) method to calculate the molecular electrostatic potential (EMP) of the tannin surface. **Fig. 2** shows the electrostatic potential maps of procyanidin, profisetidin, and prodelphinidin with HOMO and LUMO. The region's most likely to be subject to electrophilic or nucleophilic interactions are highlighted in these maps, which provide valuable information on tannin reactivity. We examined potential interaction locations using Fukui functions and Parr functions to complement the molecular electrostatic potential (MEP) results. **Fig. 2**also shows the mapping of Fukui indices for nucleophilic (f^+)and electrophilic (f^-) attacks on an electron density surface with an isovalue of 0.002.

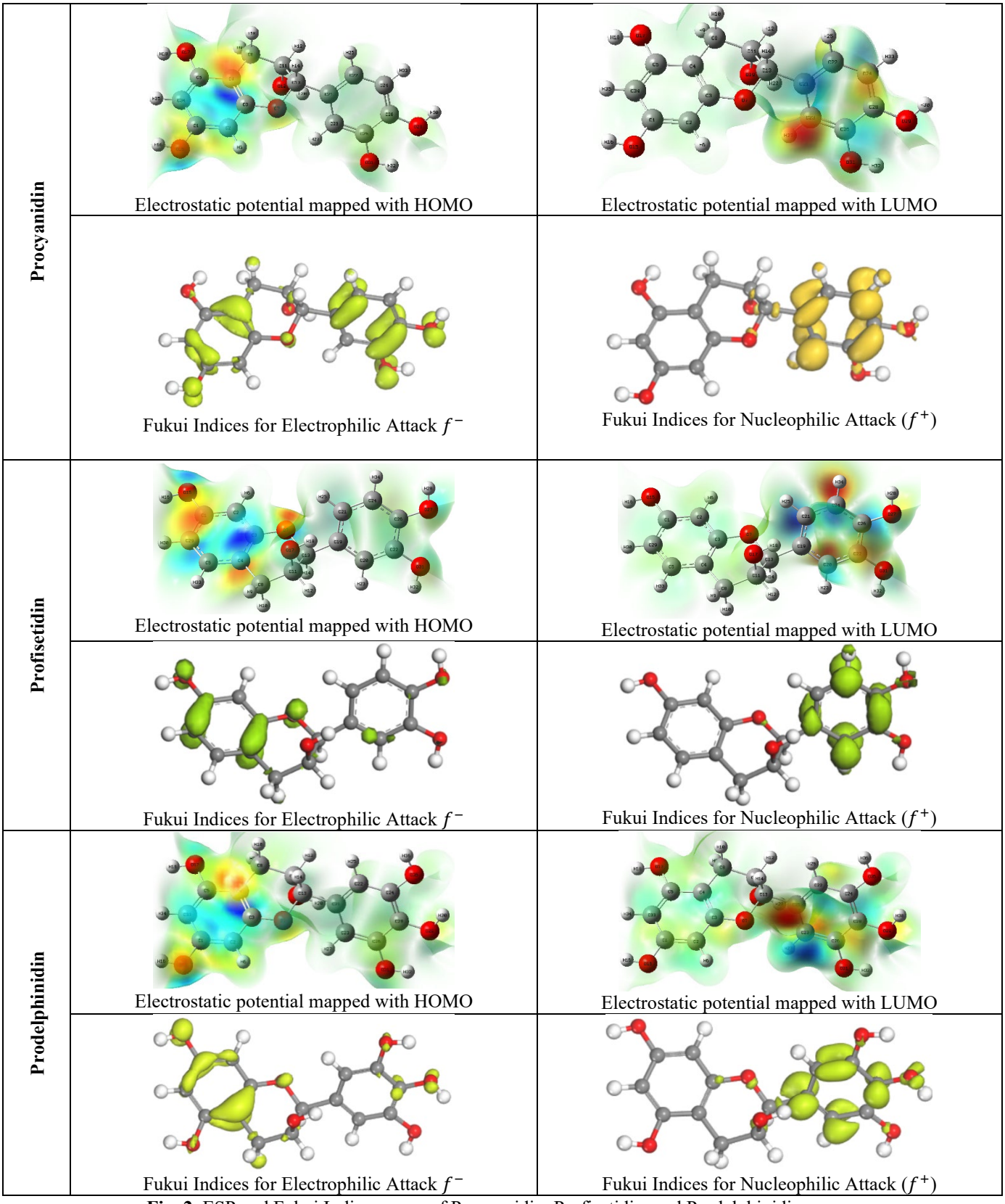

Fig. 2. ESP and Fukui Indices maps of Procyanidin, Profisetidin, and Prodelphinidin.

From the electrostatic potential surface created and represented in **Fig. 2**, we can determine where the highest electron density is found (in the reddest areas) and where the lowest electron density is found (in the darkest blue areas). For the Procyanidin molecule, the electrostatic potential mapped with HOMO is well localized on atoms C4, C22, C26, C28, O29, and O31, meaning that these sites are potentially preferable for electrophilic attack. In contrast, the electrostatic potential mapped with LUMO is localized on atoms C26, and C28, and mainly on atoms C23 and C24, meaning that these atoms are indeed preferential sites for nucleophilic attack. The mapping of Fukui index for nucleophilic (f^+) and electrophilic(f^-) attacks on an electron density surface (**Fig. 2**) and the Parr index determined by the Hirshfeld charge (**Table 2**) strongly support this finding. Following the same approach, **Table 2** and **Fig.2** show that atoms C4, O7, O15, and C29 of the Profisetidin molecule are the preferred sites for the electrophilic attack, while atoms C22, C26, and in particular C20 and C24 are the most convenient sites for the nucleophilic attack. In the Prodelphinidin molecule, the preferential sites for electrophilic attack are C4 and O15, and the most favored locations for nucleophilic attack are C21, C22, and C28.

Table 2. Local electrophilic (w^+), local nucleophilic (N^-) power, Parr Index for Electrophilic Attack(P_k^-), Parr Index for Nucleophilic Attack(P_k^+)of Procyanidin, Profisetidin, and Prodelphinidin.

	Hirshfeld index											
	Procyanidin				**Profisetidin**				**Prodelphinidin**			
Atoms	P_k^+	P_k^-	ω^+	N^-	P_k^+	P_k^-	ω^+	N^-	P_k^+	P_k^-	ω^+	N^-
C1	0.08	0.00	0.08	0.00	0.06	0.00	0.05	0.00	0.08	0.00	0.07	0.00
C2	0.02	0.00	0.02	0.00	-0.03	0.09	-0.03	0.31	0.02	0,01	0.02	0.03
C3	-0,01	0,00	-0,01	0.00	0.06	0.03	0.05	0.13	-0.02	0.09	-0.01	0.32
C4	0.33	0.00	0.30	0.00	0.28	-0,02	0,26	-0.06	0.32	0.00	0.27	0.00
C5	-0.03	0.00	-0.03	0.00	-0.10	0.12	-0.09	0.42	-0.03	0.02	-0.02	0.06
O7	0.04	0.00	0.04	0.00	0.10	0.00	0.09	0.00	0.04	0.00	0.03	0.00
C8	0.01	0.00	0.00	0.00	0.00	0.00	0.00	0.00	0.00	0.01	0.00	0.05
C11	0.01	0,00	0,01	0.00	0.02	0.00	0.02	0.00	0.01	0.01	0.01	0.05
C13	0.00	0.00	0.00	0.00	0.01	0.02	0.01	0.06	0.00	0.03	0.00	0.11
O15	0.07	0.00	0.07	0.00	0.06	0.00	0.06	0.00	0.07	0.00	0.06	0.00
O17	0.01	0.00	0.01	0.00	0.01	0.00	0.01	0.00	0.01	0.00	0.01	0.00
O19	0.01	0.03	0.01	0.11	0.05	0.04	0.04	0.16	0.01	0.00	0.01	0.00
C20	-	-	-	-	-0.02	0.29	-0.02	1.01	-	-	-	-
C21	0.05	0.05	0.04	0.17	0.05	-0.02	0.05	-0.08	0.07	0.33	0.06	1.12
C22	0.08	-0.01	0.07	-0.06	0.04	0.02	0.04	0.07	0.02	0.06	0.01	0.22
C23	-0.02	0.37	-0.02	1.27	-	-	-	-	-0.02	0.11	-0.02	0.37
C24	-0.03	0.37	-0.03	1.26	-0.02	0.26	-0.02	0.90	0.00	0.00	0.00	0.00
C26	0.07	0.05	0.07	0.17	0.07	0.07	0.07	0.25	0.04	-0.03	0.04	-0.10
O27	-	-	-	-	0.04	0.00	0.03	0.00	-	-	-	-
C28	0.09	0.07	0.08	0.26	-	-	-	-	0.13	0.24	0.10	0.82
C29	-	-	-	-	0.23	0.03	0.21	0.12	-	-	-	-
O29	0.04	0.00	0.04	0.00	-	-	-	-	0.07	0.01	0.05	0.06
O31	0.05	0.00	0.05	0.00	-	-	-	-	0.04	0.00	0.03	0.00
C33	-	-	-	-	-	-	-	-	0.06	0.05	0.05	0.20
O33					0.03	0.00	0.03	0.00	-	-	-	-
C34	0.07	0.00	0.06	0.00	-	-	-	-	-	-	-	-
O35	-	-	-	-	-	-	-	-	0.00	0.00	0.00	0.00

3.2.2 NBO Analysis

NBO analysis provides a practical basis for the study of charge transfer or conjugative interactions in molecular systems. It offers a useful approach to studying these interactions, which result in a loss of occupancy of the localized NBOs of the idealized Lewis structure to vacant non-Lewis orbitals[55].

The second-order Fock matrix was used in this study to evaluate donor-acceptor interactions based on NBO[56].These interactions lead to the transfer of electron density from NBO-filled in one subsystem to empty non-Lewis orbitals in another subsystem.

The calculations of Natural Bond Orbitals (NBOs) were performed using the Gaussian 09W software and molecular visualization program Gauss-View with CDFT/B3LYP method[57]. The purpose was to understand various second-order interactions between filled orbitals of one subsystem and vacant orbitals of another subsystem, which indicate delocalization or intermolecular hyperconjugation. Second-order perturbation theory analysis of the Fock matrix in the NBO basis was conducted, and the results are presented in **Table 3**. **Table 3** shows the occupancies and energies of i and j orbitals and the corresponding E (2) values for the LP (2) and bonding (π) to antibonding (π^*) transitions. A maximum E (2) contribution of 29.53 kcal/mol was provided by the LP (2) 15 → π^* (C1- C34) interaction for Procyanidin, Profisetidin, and Prodelphinidin molecules. The O12 → π^* (C6- C7) interaction in the Profisetidin molecule gave rise to a maximum E (2) contribution of 28.67 kcal/mol. In addition, bonding (π) and non-bonding (π^*) interactions played a substantial role in structural stability. In Procyanidin and Prodelphinidin molecules, these interactions had a maximum E (2) of 28.60 kcal/mol, while in Profisetidin molecule they had a maximum E (2) of 29.46 kcal/mol.

Table 3. Second-order Perturbation Theory Analysis of fock Matrix in NBO Basis.

Molecules	Donor	type	ED/e	acceptor	type	ED/e	E(2)	E(j)-E(i)	E(i, j)
Procyanidin	C_1-C_{34}	π	1.69394	C_2-C_3	π*	0.43031	12.87	0.29	0.056
	C_1-C_{34}	π	1.69394	C_4-C_5	π*	0.43479	26.63	0.29	0.081
	C_2-C_3	π	1.68380	C_1-C_{34}	π*	0.44321	28.21	0.28	0.081
	C_2-C_3	π	1.68380	C_4-C_5	π*	0.43479	14.37	0.29	0.059
	C_4-C_5	π	1.65810	C_1-C_{34}	π*	0.44321	14.17	0.27	0.057
	C_4-C_5	π	1.65810	C_2-C_3	π*	0.43031	28.60	0.28	0.082
	C_{21}-C_{22}	π	1.69411	C_{23}-C_{26}	π*	0.38574	18.74	0.28	0.066
	C_{21}-C_{22}	π	1.69411	C_{24}-C_{28}	π*	0.39034	19.60	0.28	0.067
	C_{23}-C_{26}	π	1.67550	C_{21}-C_{22}	π*	0.38025	20.89	0.30	0.071
	C_{23}-C_{26}	π	1.67550	C_{24}-C_{28}	π*	0.39034	19.33	0.29	0.068
	C_{24}-C_{28}	π	1.69007	C_{21}-C_{22}	π*	0.38025	18.78	0.30	0.068
	C_{24}-C_{28}	π	1.69007	C_{23}-C_{26}	π*	0.38574	19.44	0.29	0.069
	O_7	Lp(2)	1.85293	C_2-C_3	π*	0.43031	26.53	0.34	0.092
	O_{15}	Lp(2)	1.87473	C_1-C_{34}	π*	0.44321	29.53	0.34	0.098
	O_{17}	Lp(2)	1.87245	C_4-C_5	π*	0.43479	27.75	0.36	0.097
	O_{19}	Lp(2)	1.95222	C_{24}-C_{28}	π*	0.39034	26.10	0.35	0.093
	O_{31}	Lp(2)	1.87315	C_{23}-C_{26}	π*	0.38574	27.87	0.35	0.094
Profisetidin	C_1-C_4	π	1.68149	C_2-C_5	π*	0.44283	14.09	0.29	0.058
	C_1-C_4	π	1.68149	C_6-C_7	π*	0.44592	28.70	0.28	0.082
	C_2-C_5	π	1.64941	C_1-C_4	π*	0.44726	29.46	0.27	0.082
	C_2-C_5	π	1.64941	C_6-C_7	π*	0.44592	14.46	0.27	0.057
	C_6-C_7	π	1.68041	C_1-C_4	π*	0.44726	13.47	0.28	0.057
	C_6-C_7	π	1.68041	C_2-C_5	π*	0.44283	27.48	0.29	0.082
	C_{14}-C_{15}	π	1.68403	C_{16}-C_{19}	π*	0.39347	19.72	0.27	0.067
	C_{14}-C_{15}	π	1.68403	C_{17}-C_{21}	π*	0.38802	19.90	0.27	0.067
	C_{16}-C_{19}	π	1.69382	C_{14}-C_{15}	π*	0.37657	19.65	0.31	0.070
	C_{16}-C_{19}	π	1.69382	C_{17}-C_{21}	π*	0.38802	18.89	0.29	0.068
	C_{17}-C_{21}	π	1.67152	C_{14}-C_{15}	π*	0.37657	19.71	0.30	0.069
	C_{17}-C_{21}	π	1.67152	C_{16}-C_{19}	π*	0.39347	20.09	0.29	0.069
	O_9	Lp(2)	1.85351	C_1-C_4	π*	0.44726	26.73	0.34	0.092
	O_{10}	Lp(2)	1.87237	C_2-C_5	π*	0.44283	27.68	0.36	0.096
	O_{12}	Lp(2)	1.87505	C_6-C_7	π*	0.44592	28.67	0.34	0.097
	O_{23}	Lp(2)	1.87528	C_{17}-C_{21}	π*	0.38802	27.38	0.35	0.093
	O_{25}	Lp(2)	1.88773	C_{16}-C_{19}	π*	0.39347	25.90	0.36	0.092
Prodelphinidin	C_1-C_{33}	π	1.69372	C_2-C_3	π*	0.43020	12.89	0.29	0.056
	C_1-C_{33}	π	1.69372	C_4-C_5	π*	0.43486	26.63	0.29	0.081
	C_2-C_3	π	1.68408	C_1-C_{33}	π*	0.44303	28.16	0.28	0.081
	C_2-C_3	π	1.68408	C_4-C_5	π*	0.43486	14.37	0.29	0.059
	C_4-C_5	π	1.65768	C_1-C_{33}	π*	0.44303	14.18	0.27	0.057
	C_4-C_5	π	1.65768	C_2-C_3	π*	0.43020	28.60	0.28	0.082
	C_{21}-C_{23}	π	1.71726	C_{22}-C_{24}	π*	0.42372	16.13	0.28	0.062
	C_{21}-C_{23}	π	1.71726	C_{26}-C_{28}	π*	0.43200	22.12	0.27	0.072
	C_{22}-C_{24}	π	1.69043	C_{21}-C_{23}	π*	0.40663	22.33	0.30	0.074
	C_{22}-C_{24}	π	1.69043	C_{26}-C_{28}	π*	0.43200	16.99	0.28	0.064
	C_{26}-C_{28}	π	1.64809	C_{21}-C_{23}	π*	0.40663	16.80	0.30	0.064
	C_{26}-C_{28}	π	1.64809	C_{22}-C_{24}	π*	0.42372	23.33	0.29	0.075
	O_7	Lp(2)	1.85340	C_2-C_3	π*	0.43020	26.33	0.34	0.092
	O_{15}	Lp(2)	1.87469	C_1-C_{33}	π*	0.44303	29.53	0.34	0.098
	O_{17}	Lp(2)	1.87233	C_4-C_5	π*	0.43486	27.77	0.36	0.097
	O_{29}	Lp(2)	1.97494	C_{26}-C_{28}	π*	0.43200	23.36	0.35	0.088
	O_{31}	Lp(2)	1.87393	C_{26}-C_{28}	π*	0.43200	28.09	0.34	0.095
	O_{35}	Lp(2)	1.88465	C_{22}-C_{24}	π*	0.42372	26.65	0.35	0.094

4. Methods for Adsorption Localizers and Molecular Dynamics Simulations

To better understand where tannins bind to the cellulose surface and how the binding strength of the adsorbate to the substrate changes, we carried out further calculations using the adsorption localization method by performing Monte Carlo simulations on the adsorbate-substrate configuration space to identify possible adsorption configurations. This simulation method was implemented by constructing 3D cells containing a cellulose surface and a single species of tannin. The first step was to construct a crystalline cellulose lattice using PBC/3D space group symmetry and cut along the (001) plane with a thickness of 44 Å. The unit cells are then periodically replicated to combine into larger supercells with parameters a = 46.704 Å, b = 49.212 Å, and c = 44.118 Å, i.e. 6 × 6 times the original unit cell, using an empty region of 90 Å is Added periodic boundary conditions. The tannin compound optimized by CDFT/B3LYP/6-311G (d, p) calculations was imported using Materials Studio 2017 software.

4.1. Monte Carlo simulations

In order to achieve the most advantageous adsorption possible based on Monte Carlo simulations, the theoretical study in this work focuses on the interaction between tannin molecules and the cellulose surface. On the cellulose surface (001), the individual molecules are localized in the area of the surface determined by the force field values. **Figs. 3-8** show top and side views of the most stable adsorption configurations of tannin molecules attached to the surface.

Based on the donor-acceptor interactions between conjugated π-electrons and/or lone oxygen pairs in tannin molecules (side and top view), the different adsorption configurations presented in the figures3-8 show that all these molecules adsorb roughly parallel to β-Cellulose (001) (side view). Consequently, even with low concentrations of tannin, this parallel adsorption mechanism results in greater β-Cellulose (001) surface coverage.

The adsorption energy distribution for the tannin (β-Cellulose (001) system, as well as the total energy, rigid adsorption energy, deformation energy, and energy of substrate-adsorbate configurations where one of the adsorbate components has been removed, obtained by the adsorption localization module using Monte Carlo simulation, are summarized in **Table 4**. The adsorption energy is defined as the sum of the rigid adsorption energy and the deformation energy of the adsorbate components. Rigid adsorption energy corresponds to the energy released when the unstretched adsorbate components are adsorbed onto the substrate. The deformation energy represents the energy released when the adsorbent component on the substrate surface relaxes.

The values provided in **Table 1** show that the calculated adsorption energy values of the adsorption systems are all negative, meaning that adsorption could occur spontaneously. The larger negative interaction energy values can be attributed to the strong adsorption between the tannin molecules and the β-Cellulose surface (001). It is evident that the compound Prodelphinidin gives higher adsorption energy (-64.9 Kcal/mol), which means that the adsorption of this compound on the β-Cellulose (001) surface is very strong. The high adsorption energy value indicates that these tannin molecules are in fact capable of adsorbing onto the β-Cellulose (001) surface, with a very remarkable advantage for Prodelphinidin over the other molecules, namely Procyanidin and Profisetidin. This latter result confirms those found by the physical parameters affecting physical adsorption.

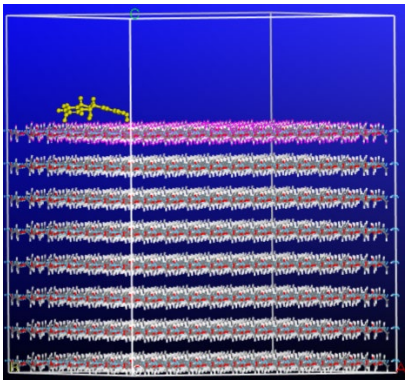

Fig. 3. Side top view of the most stable adsorption configurations of Procyanidin over β-Cellulose (001) surface

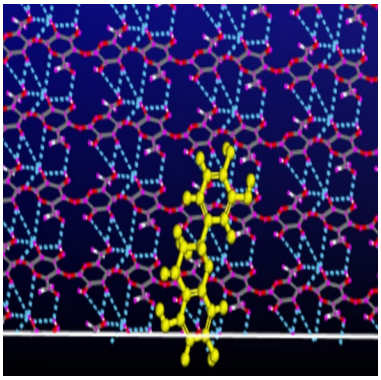

Fig. 4. Top view of the most stable adsorption configurations of Procyanidin over β-Cellulose (001) surface

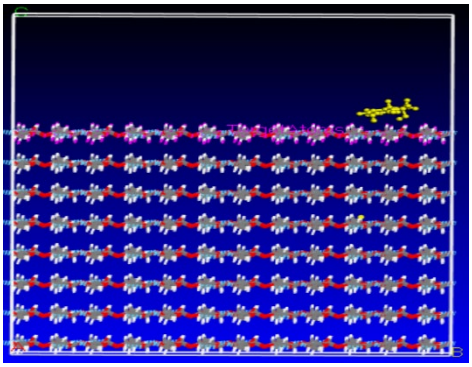

Fig. 5. Side top view of the most stable adsorption configurations of Profisetidin over β-Cellulose (001) surface

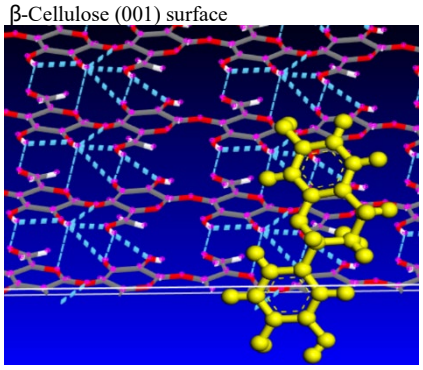

Fig. 6. Top view of the most stable adsorption configurations of Profisetidin over β-Cellulose (001) surface

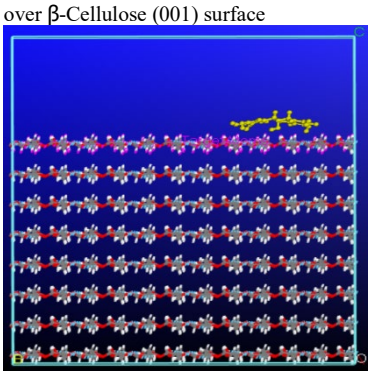

Fig. 7. Side top view of the most stable adsorption configurations of Prodelphinidin over β-Cellulose (001) surface

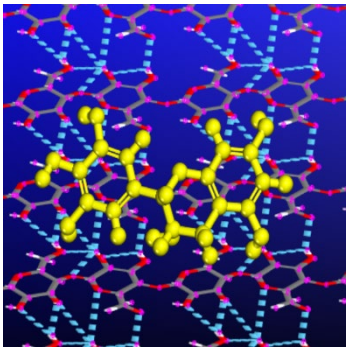

Fig. 8. Top view of the most stable adsorption configurations of Prodelphinidin over β-Cellulose (001) surface

Table 4. Adsorption energies for tannin (1-3) compounds on the β-Cellulose surface (Kcal/mol).

Structures	Total Energy	Adsorption Energy	Rigid Adsorption	Deformation Energy ($\times 10^{-10}$)	dE_{TANNIN}/dN_i
Procyanidin-β-Cellulose	-31.7	-57.4	-62.0	4.6	-57.4
Profisetidin-β-Cellulose	-76.4	-62.2	-61.1	-1.0	-62.2
Prodelphinidin-β-Cellulose	-90.0	-64.9	-68.5	3.6	-64.9

4.2. RDF Functions

The probability of finding a particle A at a distance r from a particle B is expressed by the radial distribution function (RDF), defined by the equation (19)[58,59]. In other words, it explains how the density of the region around a point varies with distance. The RDF is highly dependent on the type of material. Consequently, it differs considerably for solids, gases, and liquids. It provides data on the frequency of occurrence of a particular distance. RDF curves reflecting crystalline structures can show significant peaks, as can X-ray diffraction (XRD) curves, demonstrating that a certain interatomic spacing is frequently present in the structure. It can be expressed as shown above by the density of the species averaged over all shells around the species.

$$g_{AB}(r) = \frac{1}{\langle \rho_B \rangle_{local}} \times \frac{1}{N_A} \sum_{i \in A}^{N_A} \sum_{j \in B}^{N_B} \frac{\delta(r_{ij} - r)}{4\pi r^2} \tag{19}$$

In this section, the radial distribution function (RDF) was used as a method of calculating the distance between tannin molecules and the β-Cellulose surface (001). **Figs. (9-11)** show the calculated RDF plot of the simulated model[58,60,61]. A strong, sharp peak is observed at a distance of 1.15 Å, and another moderately strong peak at a distance of 3.9Å. Note that if the distance between adsorbate and adsorbent is between 1Å and 3.5Å, Coordination bonds are present or strong hydrogenated bonds resulting from the overlap between the mimosa atoms of the tannins and the β-cellulose surface (001), which in turn contains several O-H bonds. Beyond 3.5 Å, interactions are governed by electrostatic and/or Van Der Waals-type interactions.

All three molecules of tannins were adsorbed on the cellulose surface in the same way (001). According to the analysis in **Figs. (9-11)**, two types of adsorption govern the adsorption mode: Physisorption, which involves weak van der Waals bonds between the adsorbed chemical species and the adsorbent, and chemisorption, which involves strong covalent bonds. The bond lengthdistribution of the three molecules on the β-Cellulose surface confirms this result (**Figs. 12-14**).

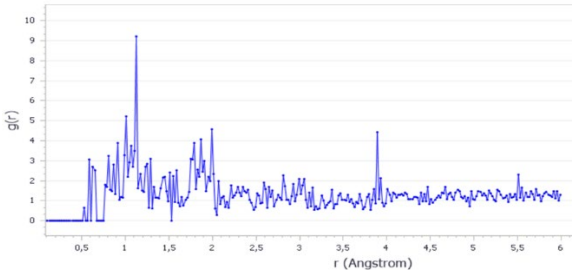

Fig. 9. Radial distribution function between Procyanidin and β-Cellulose (001) surface.

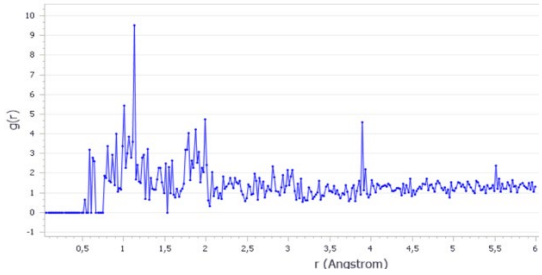

Fig. 10. Radial distribution function between Profisetidin and β-Cellulose (001) surface.

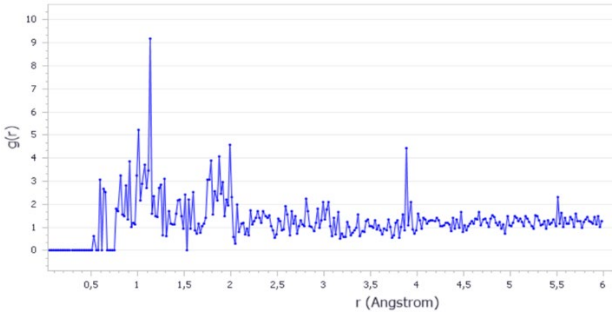

Fig. 11. Radial distribution function between Prodelphinidin and β-Cellulose (001) surface.

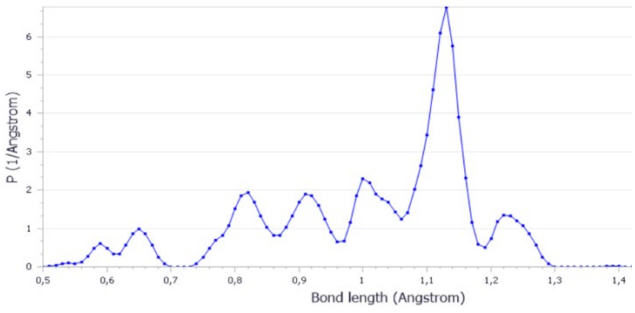

Fig. 12. Bond lengths such as Procyanidin- β-Cellulose (001) surface.

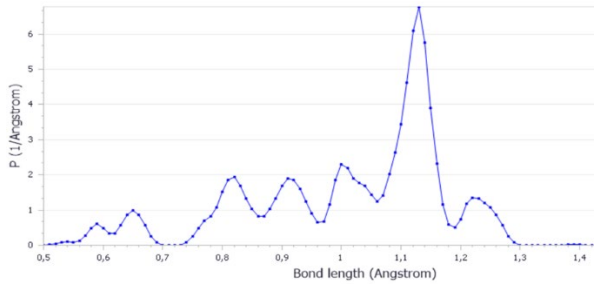

Fig. 13. Bond lengths such as Profisetidinβ-Cellulose (001) surface.

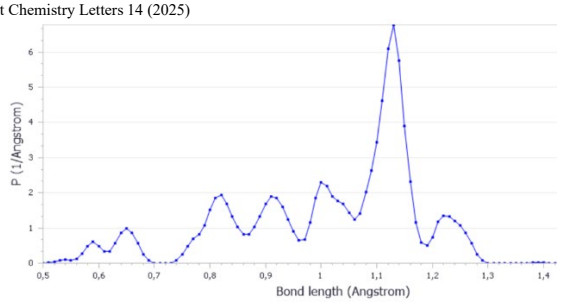

Fig. 14. Bond lengths such as Prodelphinidin- β-Cellulose (001) surface.

5. Conclusion

In conclusion, this theoretical and computational study sheds light on the adsorption behavior of tannins on cellulose surfaces, which is crucial for sustainable wood adhesives. It employs advanced calculations, Monte Carlo simulations, and molecular dynamics to analyze the interactions of tannins with wood.

The results highlight the pivotal role of donor-acceptor interactions, particularly prodelphinidin with strong adsorption energy, showing promise for eco-friendly adhesives. Polarity and polarizability also play a significant role in the adsorption process, offering insights into effective adhesive formulations.

All tannin compound molecules adhered completely parallel to the cellulose surface via electron transfer interactions with high negative adsorption energy, according to Monte Carlo annealing simulated using the adsorption localization module and quantum mechanical simulations. The MC simulation revealed that prodelphinidin has a higher negative adsorption energy, with the most stable configuration at 293 K corresponding to an adsorption energy value of -64.92 Kcal/mol.This research supports the reduction of formaldehyde emissions in the wood industry by harnessing asome different kinds of tannins coming from different origins. It paves the way for sustainable adhesives, aligning with environmentally-friendly industry practices in different fields as reported before in a lot of scientific papers[62-67].

Funding

This research received no external funding.

Declaration of Competing Interest

The authors declare that they have no known competing financial interests or personal relationships that could have appeared to influence the work reported in this paper.

Data availability

No data was used for the research described in the article.

References

1. Moubarik, A., Charrier, B., Allal, A., Charrier, F., & Pizzia, A. (**2010**). Development andOptimization of a New Formaldehyde-Free Cornstarch and Tanninwood Adhesive. *Eur. J. Wood Wood Prod.68* (2), 167–177. https://doi.org/10.1007/s00107-009-0357-6.
2. Pizzi, A. (**1979**). The Chemistry and Development of Tannin/Urea–Formaldehyde Condensates for Exterior Wood Adhesives. *J. Appl. Polym. Sci.23* (9), 2777–2792. https://doi.org/10.1002/app.1979.070230922.
3. Pizzi, A. P. (**1979**). Industrial Application of Wattle Tannin / Urea-Formaldehyde Fortified Starch Adhesives for Damp-Proof Corrugated Cardboard. *Holzforsch. und Holzverwertung6* (February), 131–133.
4. Garcia, R., & Pizzi, A. (**1998**). Polycondensation and Autocondensation Networks in Polyflavonoid Tannins. I. Final Networks. *J. Appl. Polym. Sci.70* (6), 1083–1091. https://doi.org/10.1002/(sici)1097-4628(19981107)70:6<1083::aid-app5>3.3.co,2-w.
5. Gonçalves, F. G., Lelis, R. C. C., & Da Silva Oliveira, J. T. (**2008**). Influence of the Composition of Tannin-Urea-Formaldehyde Resins in the Physical and Mechanicals Properties of Particleboard. *Rev. Arvore32* (4), 715–722. https://doi.org/10.1590/s0100-67622008000400013.
6. Zhou, X., & Du, G. (**2020**). Applications of Tannin Resin Adhesives in the Wood Industry. *Tann. - Struct. Prop. Biol. Prop. Curr. Knowl.* 1–19. https://doi.org/10.5772/intechopen.86424.
7. Moubarik, A., Pizzi, A., Allal, A., Charrier, F., Khoukh, A., & Charrier, B. (**2010**). Cornstarch-Mimosa Tannin-Urea Formaldehyde Resins as Adhesives in the Particleboard Production. *Starch/Staerke62* (3–4), 131–138. https://doi.org/10.1002/star.200900228.

8. Moubarik, A., Pizzi, A., Charriera, F., Allala, A., Badia, M., Mansouri, H. R., & Charrier, B. (**2013**). Mechanical Characterization of Industrial Particleboard Panels Glued with Cornstarch-Mimosa Tannin-Urea Formaldehyde Resins. *J. Adhes. Sci. Technol.27* (4), 423–429. https://doi.org/10.1080/01694243.2012.711739.
9. Ping, L., Brosse, N., Chrusciel, L., Navarrete, P., & Pizzi, A. (**2011**). Extraction of Condensed Tannins from Grape Pomace for Use as Wood Adhesives. *Ind. Crops Prod.33* (1), 253–257. https://doi.org/10.1016/j.indcrop.2010.10.007.
10. Chakraborty,D., & Chattaraj,P. K. (**2021**). Conceptual density functional theory based electronic structure principles. *Chem. Sci.12*, 6264–6279. DOI: 10.1039/d0sc07017c.
11. Domingo, L. R., & Pérez, P. (**2013**). Global and Local Reactivity Indices for Electrophilic/Nucleophilic Free Radicals. *Org. Biomol. Chem.11* (26), 4350–4358. https://doi.org/10.1039/c3ob40337h.
12. Mendoza-Huizar, L. H. (**2015**). Global and Local Reactivity Descriptors for Picloram Herbicide: A Theoretical Quantum Study. *Quim. Nova38* (1), 71–76. https://doi.org/10.5935/0100-4042.20140283.
13. Brandán A. S. (**2017**). Vibrational Characterization Of Monomers And Dimers Of Cellulose By Using Dft Calculations And The Sqm Methodology.*SDRP J. Comput. Chem. Mol. Model.* https://doi.org/10.15436/JCCMM.1.2.4.
14. M. J. Frisch, G. W. Trucks, H. B. Schlegel, G. E. Scuseria, M. A. Robb, J. R. Cheeseman, V. G. Zakrzewski, J. A. Montgomery Jr., R. E. Stratmann, J. C. Burant, S. Dapprich, J. M. Millam, A. D. Daniels, K. N. Kudin, M. C. Strain, O. Farkas, J., & Tomasi, V. B, J. A. P. Gaussian 98, Revision A.6, Gaussian, Inc., Pittsburgh, PA. 2003.
15. Atoms, D. T., Parr, M. R. G., & Yang, W. (**1989**). Book Review. *Density Funct. Theory Atoms Mol.47*, 10101.
16. Geerlings, P., De Proft, F., Langenaeker, W. (**2003**).Conceptual Density Functional Theory. *Chem. Rev.103* (5), 1793–1873. https://doi.org/10.1021/cr990029p.
17. Chattaraj, P. K., Duley, S., & Domingo, L. R. (**2012**). Understanding Local Electrophilicity/Nucleophilicity Activation through a Single Reactivity Difference Index. *Org. Biomol. Chem.10* (14), 2855–2861. https://doi.org/10.1039/c2ob06943a.
18. Becke, A. D. (**1993**). A New Mixing of Hartree-Fock and Local Density-Functional Theories. *J. Chem. Phys.98* (2), 1372–1377. https://doi.org/10.1063/1.464304.
19. Becke, A. D. (**1992**). Density-functional Thermochemistry. I. The Effect of the Exchange-only Gradient Correction. *J. Chem. Phys.96* (3), 2155–2160. https://doi.org/10.1063/1.462066.
20. Chengteh Lee, & Weitao Yang, R. G. P. (**1987**). Development of the Colic-Salvetti Correlation-Energy into a Functional of the Electron Density. *Phys. REVIE B37* (2), 785–789.
21. Bakowies, D., & von Lilienfeld,O. A.(**2021**). Density Functional Geometries and Zero-Point Energies in Ab Initio Thermochemical Treatments of Compounds with First-Row Atoms (H, C, N, O, F). J. *Chem. Theory Comput.17*, 4872−4890.
22. Plumley, J. A., & Dannenberg, J.J.(**2011**).A Comparison of the Behavior of Functional/Basis Set Combinations for Hydrogen-Bonding in the Water Dimer with Emphasis on Basis Set Superposition Error.*J Com put Chem.32*(8), 1519–1527. doi:10.1002/jcc.21729.
23. Tirado-Rives, J. L., & Jorgensen,W.(**2008**). Performance of B3LYP Density Functional Methods for a Large Set of Organic Molecules. *J. Chem.Theory Comput.4*, 297-306.
24. Deb, B. M. (**1975**). Additions and Corrections: A Simple Mechanical Model for Molecular Geometry Based on the Hellmann-Feynman Theorem. I. General Principles and Applications to AH2, AH3, AH4, AB2, HAB and ABC Molecules. *J. Am. Chem. Soc.97* (7), 1988. https://doi.org/10.1021/ja00840a611.
25. Pearson, R. G. (**1986**). Absolute Electronegativity and Hardness Correlated with Molecular Orbital Theory. *Proc. Natl. Acad. Sci.83* (22), 8440–8441. https://doi.org/10.1073/pnas.83.22.8440.
26. Pearson, R. G. (**1999**). Maximum Chemical and Physical Hardness. *J. Chem. Educ.76* (2), 267–275. https://doi.org/10.1021/ed076p267.
27. Pearson, R. G. (**1987**). Recent Advances in the Concept of Hard and Soft Acids and Bases. *J. Chem. Educ.64* (7), 561–567. https://doi.org/10.1021/ed064p561.
28. Parr, R. G., Donnelly, R. A., Levy, M., & Palke, W. E. (**1977**).Electronegativity: The Density Functional Viewpoint. *J. Chem. Phys.68* (8), 3801–3807. https://doi.org/10.1063/1.436185.
29. Edition, S., Koch, W., Holthausen, M. C., *Wolfram Koch , Max C* .(**2001**). *Holthausen A Chemist's Guide to Density Functional Theory*, Vol. 3.
30. Parr, R. G., & Pearson, R. G.(**1983**). Absolute Hardness: Companion Parameter to Absolute Electronegativity. *J. Am. Chem. Soc.105* (26), 7512–7516. https://doi.org/10.1021/ja00364a005.
31. Pratihar, S., & Roy, S.(**2010**). Nucleophilicity and site selectivity of commonly used arenes and heteroarenes.*J. Org. Chem. 75*, 4957–4963.
32. Gázquez, J. L., Cedillo, A., & Vela, A. (**2007**). Electrodonating and Electroaccepting Powers. *J. Phys. Chem. A.111* (10), 1966-1970, DOI: 10.1021/jp065459f.
33. Yang, W., & Parr, R. G.(**1985**). Hardness, Softness, and the Fukui Function in the Electronic Theory of Metals and Catalysis. *Proc. Natl. Acad. Sci. U. S. A.82* (20), 6723–6726. https://doi.org/10.1073/pnas.82.20.6723.
34. Parr, R. G., Szentpály, L. V., & Liu, S. (**1999**). Electrophilicity Index. *J. Am. Chem. Soc.121* (9), 1922–1924. https://doi.org/10.1021/ja983494x.
35. Chattaraj, P. K., & Giri, S.(**2009**). Electrophilicity Index within a Conceptual DFT Framework. *Annu. Reports Prog. Chem. - Sect.c,105*, 13–39. https://doi.org/10.1039/b802832j.
36. Chattaraj, P. K., & Roy, D. R.(**2007**). Update 1 of: Electrophilicity Index. *Chem. Rev.107* (9), PR46–PR74.

https://doi.org/10.1021/cr078014b.
37.Amini,L., El Karni, H., Oubenali, M., EL Ouafy, H., Mbarki, M., & El Ouadi, B.(**2024**). Predictive study, using density functional theory and time dependent functional theory, on the structure-property quantification of methylene blue and methyl red dyes for the application in organic solar cells. *Curr. Chem. Lett. 13*, 187–198.
38.AND, W. K., SHAM, L. J.(**1965**). Self-Consistent Equations Including Exchange and Correlation Effects. *Phys. Rev.140*, A 1133-A 1138.
39.Domingo, L. R., Chamorro, E., & Pérez, P. (**2008**). Understanding the Reactivity of Captodative Ethylenes in Polar Cycloaddition Reactions. A Theoretical Study. *J. Org. Chem.73* (12), 4615–4624. https://doi.org/10.1021/jo800572a.
40.Domingo, L. R., & Pérez, P.(**2011**).The Nucleophilicity N Index in Organic Chemistry. *Org. Biomol. Chem.9* (20), 7168–7175. https://doi.org/10.1039/c1ob05856h.
41.Domingo, L. R., & Picher, M. T.(**2004**). A DFT Study of the Huisgen 1,3-Dipolar Cycloaddition between Hindered Thiocarbonyl Ylides and Tetracyanoethylene. *Tetrahedron60* (23), 5053–5058. https://doi.org/10.1016/j.tet.2004.04.024.
42.Berger, G.(**2013**). Using Conceptual Density Functional Theory to Rationalize Regioselectivity: A Case Study on the Nucleophilic Ring-Opening of Activated Aziridines. *Comput. Theor. Chem.1010*, 11–18. https://doi.org/10.1016/j.comptc.2012.12.029.
43.Morell, C., Grand, A., & Toro-Labbé, A.(**2006**). Theoretical Support for Using the Δf(r) Descriptor. *Chem. Phys. Lett.425* (4–6), 342–346. https://doi.org/10.1016/j.cplett.2006.05.003.
44.Parr, R. G., & Yang, W.(**1984**).Density Functional Approach to the Frontier-Electron Theory of Chemical Reactivity. *J. Am. Chem. Soc.106* (14), 4049–4050. https://doi.org/10.1021/ja00326a036.
45.Domingo, L. R., Aurell, M. J., Pérez, P., & Contreras, R.(**2002**).Quantitative Characterization of the Local Electrophilicity of Organic Molecules. Understanding the Regioselectivity on Diels-Alder Reactions. *J. Phys. Chem. A*, *106* (29), 6871–6875. https://doi.org/10.1021/jp020715j.
46.Pérez, P., Domingo, L. R., Duque-Noreña, M., & Chamorro, E.(**2009**).A Condensed-to-Atom Nucleophilicity Index. An Application to the Director Effects on the Electrophilic Aromatic Substitutions. *J. Mol. Struct. THEOCHEM* , *895* (1–3), 86–91. https://doi.org/10.1016/j.theochem.2008.10.014.
47.Akkermans, R. L. C., Spenley, N. A., & Robertson, S. H.(**2013**). Monte Carlo Methods in Materials Studio. *Molecular Simulation*. Taylor & Francis, pp 1153–1164. https://doi.org/10.1080/08927022.2013.843775.
48.2017, M. S.(**2017**). Materials Studio, Revision 8.0, Accelrys Inc., San Diego, USA.
49. Zakaria, J., Karni, E., Hassan, E., EL Ouafy, T., Echajia, M., Mohamed, M., & Oubenali, M. (**2023**). Reactivity of Isothiasole with Dibromine and Sulfuryl Chloride. *Phys. Chem. Res.11* (3), 511-525. DOI: 10.22036/pcr.2022.341501.2098.
50. Jalil, Z ., El Karni, H., Touil, M., Mbarki, M., & Oubenali, M. (**2025**). The quantum chemical study of the reaction between chlorocarbonylsulfenyl chloride and benzamide. *Curr. Chem. Lett. 14*, 21–30.
51. Domingo, L.R., Pérez,P., & Sàez, J. (**2013**). Understanding thelocal reactivity in polar organic reactions through electrophilic and nucleophilic Parr functions. *RSC Advences.3*,1486-1496. DOI: 10.1039/c2ra22886f.
52. El Assyry, A., Touil,M.,Benhiba, F., Benali, B., Rabaâ, H., Lakhrissi, B., Warad, I., Bentiss, F., & Zarrouk, A.(**2020**). Computational Simulation of the AdsorptionBehavior of Benzimidazolone Derivatives as Inhibitors for Ordinary Steel Corrosion in HCl 1M.*Anal. Bioanal. Electrochem.12*(5), 580-606
53. Denis, J., Jean-Marie, A., Eric, A. P. (**2004**). Geometry, dipole moment, polarizability and first hyperpolarizability of polymethineimine: An assessment of electron correlation contributions. *J. Chem. Physi.* 121(9), 4389-4396.
54. Krishna Kumar,V., Sangeetha, R., Barathi, D., Mathammal, R., & Jayamani, N. (**2014**). Vibrational assignment of the spectral data, molecular dipole moment, polarizability, first hyperpolarizability, HOMO–LUMO and thermodynamic properties of 5-nitoindan using DFT quantum chemical calculations. *Spectrochim. Acta. A. Mol. Biomol. Spectrosc.*118, 663-671.
55. Singh, R. N., Kumar, A., Tiwari, R. K., Rawat, P., & Gupta, V. P. (**2013**). A combinedexperimental and quantum chemical (DFT and AIM) study on molecular structure,spectroscopic properties, NBO and multiple interaction analysis in a novel ethyl 4-[2- (carbamoyl)hydrazinylidene]-3,5-dimethyl-1H-pyrrole-2-carboxylate and its dimer. *J. Molestruc.1035*, 427–440.doi:10.1016/j.molstruc.2012.11.059
56.Weinhold, F., Landis, C. R., & Reed, A. E. (**2001**). Intermolecular Interactions from a Natural Bond Orbital , Donor-Acceptor Viewpoint *Chem. Educ. Res. Pr.2* (September 1988), 91–104.
57.(**2009**).GaussView, Version 5, Roy Dennington, Todd Keith and John Millam, Semichem Inc., Shawnee Mission KS.
58.Wang, W., Li, Z., Sun, Q., Du, A., Li, Y., Wang, J., Bi, S., & Li, P. (**2012**).Insights into the Nature of the Coupling Interactions between Uracil Corrosion Inhibitors and Copper: A DFT and Molecular Dynamics Study. *Corros. Sci.61*, 101–110. https://doi.org/10.1016/j.corsci.2012.04.025.
59.Chandler, D., Percus, J. K.(**1988**).*Introduction to Modern Statistical Mechanics* , Vol. 41. https://doi.org/10.1063/1.2811680.
60.Fouda, A. S., Ismail, M. A., Abousalem, A. S., & Elewady, G. Y.(**2017**). Experimental and Theoretical Studies on Corrosion Inhibition of 4-Amidinophenyl-2,2′-Bifuran and Its Analogues in Acidic Media. *RSC Adv.7* (73), 46414–46430. https://doi.org/10.1039/c7ra08092a.
61.Emregül, K. C., & Atakol, O.(**2004**). Corrosion Inhibition of Iron in 1 M HCl Solution with Schiff Base Compounds and Derivatives. *Mater. Chem. Phys.83* (2–3), 373–379. https://doi.org/10.1016/j.matchemphys.2003.11.008.

62. Elhady, O., Mansour, E., Elwassimy, M., Zawam, S., & Drar, A. (2022). Synthesis and characterization of some new tebufenozide analogues and study their toxicological effect against Spodoptera littoralis (Boisd.). *Curr. Chem. Lett.*, *11*(1), 63-68.
63. El Tabl, A., Zawam, S., & Sarhan, K. (**2021**). Innovatingnewmethods for wastewater treatment in El-Dakhla Oasis in Upper Egypt fromchemical and biological pollutants using modified down Flow Hanging Sponge(DHS) reactor in presence of new environmental friendly chelator. *Egypt. J. Chem.64*(9), 4985–4994.
64. A. A. Abdel-Raheem,S ., Ali M. Drar., Bahgat R. M. Hussein.,Amr H.Moustafa.(**2023**).Some oxoimidazolidine and cyanoguanidine compounds: Toxicological efficacy and structure-activity relationships studies. *Curr. Chem. Lett*. 12(4), 695–704.
65. Fouad M. R., Abd-Eldaim F. A., Alsehli B. R., Mostafa A. S.**(2024**). Noncompetitive and competitive sorption of imidacloprid and KNO3 onto soils and their effects on the germination of wheat plants (Triticum aestivum L.). *Global Nest Journal*. 26(5), 05670.
66. Faten Anwar, A., Khaed Yehia, F., Fatma Said, S., Mohamed Riad, F., Omaima Saleh, D., Sekina Sayed, E., & Khaled Yassin, A. (**2023**). Phytotoxic effects of ımidacloprid and its nano-form on the cucumber plants under greenhouse condition and their toxicity on HepG2 cell line. *Arch. Phytopathol. Pflanzenschutz., 56*(19), 1467–1486.
67. Drar, A. M., A. A. Abdel-Raheem, S., Moustafa, A. H., & Hussein, B. R. M. (**2023**). Studying the toxicity and structure-activity relationships of some synthesized polyfunctionalized pyrimidine compounds as potential insecticides. *Curr. Chem. Lett. 12*(3), 499–508.